<Original Paper> Journal of the Korean Society for Nondestructive Testing, Vol. 34, No. 6: 441-446, 2014
ISSN 1225-7842 / eISSN 2287-402X http://dx.doi.org/10.7779/JKSNT.2014.34.6.441

2D Sparse Array Transducer Optimization for 3D Ultrasound Imaging

Jae Hoon Choi* and Kwan Kyu Park*†

Abstract A 3D ultrasound image is desired in many medical examinations. However, the implementation of a 2D array, which is needed for a 3D image, is challenging with respect to fabrication, interconnection and cabling. A 2D sparse array, which needs fewer elements than a dense array, is a realistic way to achieve 3D images. Because the number of ways the elements can be placed in an array is extremely large, a method for optimizing the array configuration is needed. Previous research placed the target point far from the transducer array, making it impossible to optimize the array in the operating range. In our study, we focused on optimizing a 2D sparse array transducer for 3D imaging by using a simulated annealing method. We compared the far-field optimization method with the near-field optimization method by analyzing a point-spread function (PSF). The resolution of the optimized sparse array is comparable to that of the dense array.

Keywords: Sparse Array Transducer, Simulated Annealing, Optimization, Ultrasound 3D Imaging

1. Introduction

The conventional ultrasound transducer array is typically fabricated in one-dimension (1D) array configuration. It can image only two dimensional (2D) B-mode image. The inspection area of B-mode image depends on the transducer direction, i.e. the imaging plane is made by the lateral direction and the perpendicular direction of the transducer array. In order to expend the 2D imaging plane to 3D imaging volume, 2D transducer array is necessary. One example of 3D array is N by N dense array, which consists of N^2 elements. However, 2D dense array is challenging in terms of fabrication, interconnections and cabling. Alternative method for constructing 3D image is the 2D sparse array. The 2D sparse array locates less number of elements in a 2D grid space. As a results, the distance between each elements will be larger than that of the size of the element. The sparse array's objective is constructing 3D image as similar as the image from the 2D dense array.

The 2D sparse array configuration can be a variety of shapes as shown in Fig. 1. The left figures are the array configuration in 2D space and the right figures are corresponding simulated C-mode images, which are the parallel plane image to the transducer, with one point target in on-axis. The transducer's elements' position have a tremendous impact on the image quality. If elements' are located properly, the image quality of the sparse array can be comparable to that of the 2D dense array. However, the number of case locating elements is closed to infinity [1, 2]. Therefore, an optimized method for array configuration is required.

2. Optimization Method

We used a simulated annealing method to find the best sparse array. The optimization method finds a global minimum by accepting new solution with some probability. This method has four steps: generating new solution, calculating

[Received: November 12, 2014, Revised: December 14, 2014, Accepted: December 16, 2014] *Department of Mechanical Convergence Engineering, Hanyang University, Seoul 133-791, Korea †Corresponding Author: kwankyu@hanyang.ac.kr

objective function, updating the solution and decreasing the temperature.

2.1 Generating New Solution

First process of the simulated annealing is generating new solution, which is the locations of elements. In N-by-N 2D grid space, we randomly located M elements. The new solution was the initial state of the optimization method. The next solution is defined by changing the location of randomly selected one element by one grid space.

2.2 Calculating Objective Function

To evaluating how much better or worse the new solution is, we constructed the C-mode image with one point target, i.e. point-spread function(PSF). In the C-mode image, the desired signal, main lobe, exists near the target point and undesired signal, side lobe, exists out of the point's position. Therefore, we defined an objective function (Eq.1) as the ratio of the sum of side lobe and the sum of main lobe. The optimization objective is the minimizing this function.

$$F_i = \frac{sum\ of\ sidelobe}{sum\ of\ mainlobe} \tag{1}$$

2.3 Updating the Solution

We should determine whether the new solution is accepted or not. If the objective function of the new solution is lower than that of the previous solution, the new solution must be accepted. If the objective function of the new solution is higher than the previous solution, the acceptance probability of the new solution is calculated and the calculated probability determines whether the solution is accepted or not. The probability of acceptance is tabulated in Table 1.

Table 1 The probability ff accepting the new solution

$If \ \ \triangle F_i < 0$	$P_{accept} = 1$
$If \ \ \triangle F_i > 0$	$P_{accept} = e^{-\frac{\triangle F_i}{T}}$

Where, $\triangle F_i = F_i - F_{i-1}$, $T: tem\ perature$

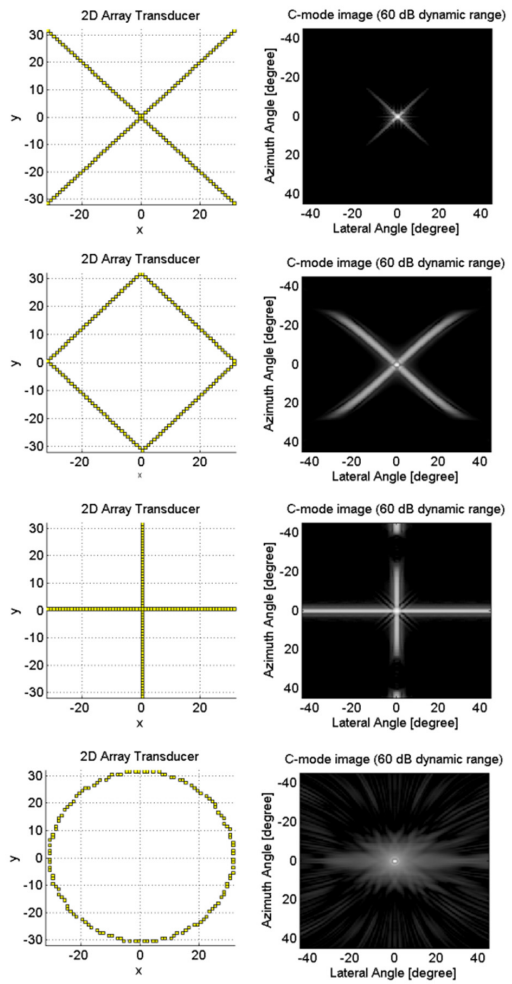

Fig. 1 Examples of sparse array configuration and their C-mode image: (left) top view of spare array, (right) C-mode image

2.4 Decreasing the Temperature

In early iterations, the probability of accepting the worse solution should be high, since the probability of falling in local minimum is high. On the other hands, in late iterations, the

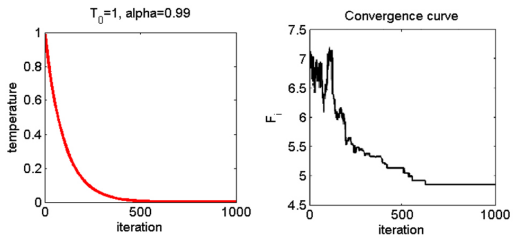

Fig. 2 (left) temperature curve, (right) objective function curve

accepting probability should be low, because the probability of falling in global minimum is high. To address the logic, we controlled the temperature, which becomes lower as the optimization is repeated. It is expressed as follows:

$$T = T_0 \times \alpha^i \quad , \tag{2}$$

where, T_0 is initial temperature, α is cooling factor, and i is the number of iteration.

The probability of accepting solution is calculated based on Eq. (2). In this work, we set the initial temperature to be 1, and the cooling factor to be 0.99. The temperature curve of iteration number is presented in Fig. 2. As shown in the Fig 2, the temperature decreases as iterations goes. The probability of the accepting solution is strongly correlated with the temperature. The objective function curve (F_i) of iteration number is presented in Fig. 2. In the early iterations, the objective function varies a lot. It means that the solution looks for the global minimum and escapes local minima in the early iterations. On the other hand, in the late iterations, the objective function is converged some value. It can be considered as falling in the global minimum. Multiple simulated annealing calculations were performed and the results presented slightly different patterns of sparse array configurations. However, their objective function values (F_i) of arrays are very similar to each other. Therefore, this method is valid to find one of global minima.

3. Simulation Condition

In previous researches [2,3], a point target is assumed to be located in infinitely far distance from a transducer array. In the approach, the point spread function (PSF) can be calculated by an analytical method [4]. However, it does not guarantee that the solution is optimized for the imaging of the actual operating range of the transducer. To address this issue, we considered two cases. In the first case, the array is optimized for the point target located at the distance of one hundred times of array size (far-field optimization). This approach is similar to the previous works [2,3]. In the second case, the array is optimized for the point target at the distance of five times of array size (near-field optimization). The PSF image of two cases were compared to the image from a dense array of the same aperture size. In this work, we used phase array imaging for the calculation of PSF.

Simulation conditions are tabulated at Table 2. The element size is the half of the wave length. The kerf which is the distance between two elements is a fifth of elements size. The 128 elements are placed in 64 by 64 element grid space (M=128, N=64). Array size is the length of 64 elements and kerf. We use mirrored image of quadratic array to prevent asymmetric side lobes. The solution is converged after 1000 iterations.

Table 2 Simulation conditions

Center frequency	5 MHz
Ultrasound velocity	1540 m/s
Element size	154 μm
Kerf	30.8 μm
Array size	11.8 mm
Initial temperature	1
Cooling factor	0.99

4. Simulation Results

Optimized array configurations are presented in Fig. 3. In order to evaluate the performance of the sparse arrays, we constructed image of a point target at the distance of the five times of array size as shown in Fig. 4. The B-mode image is the vertical plane image of the transducer array and the C-mode image is the parallel plane image.

As expected, Fig. 4 clearly indicates superior image quality of the dense array with a cost of a large element number (M=4096). However, the optimized sparse arrays presented similar resolution at the main lobe. However, it is technically hard to compare the two sparse array by visual inspection of B-mode and C-mode images.

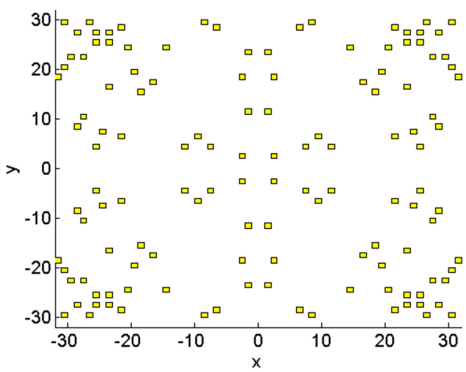

(a) elements positions on the far field optimization

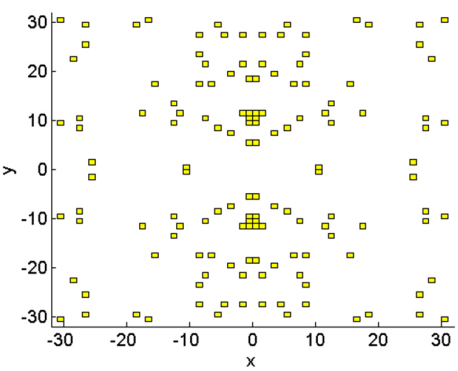

(b) elements positions on the near field optimization

Fig. 3 Array configuration: (a) far field optimization, (b) near field optimization

In order to quantify the image quality we made five evaluation indicators. Integrated Side lobe Ratio (ISLR) is the first indicators [5]. ISLR is the measure of the ratio of sum of side lobe and sum of main lobe. In addition, the maximum value of the size lobe (side lobe peak) and the total energy of the side lobe (side lobe sum) are use as the evaluation indicators [6]. In the evaluation of the side lobes of the sparse array, the area of the side lobes is based on that of the dense array, which is presented in Fig. 5. This approach prevents the sparse array gather more energy in the main lobe by sacrificing the resolution of the PSF. Other two indicators are 3-dB resolution of the PSF in both later and axial directions.

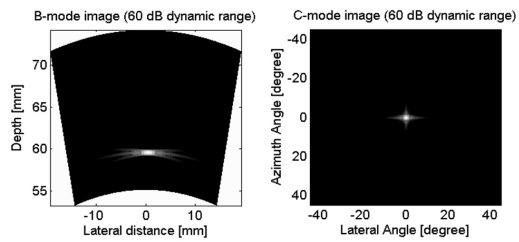

(a) dense array

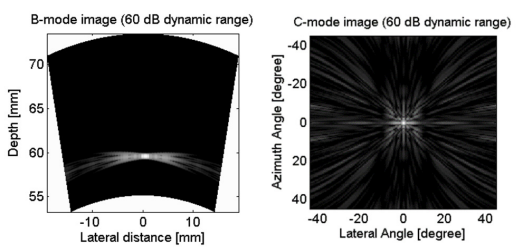

(b) far field optimization

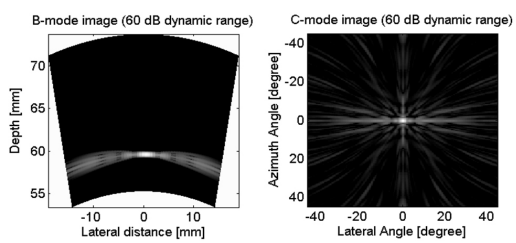

(c) near field optimization

Fig. 4 Simulation result of (left) B-mode image and (right) C-mode image. The point target is at the distance of five times of the transducer size

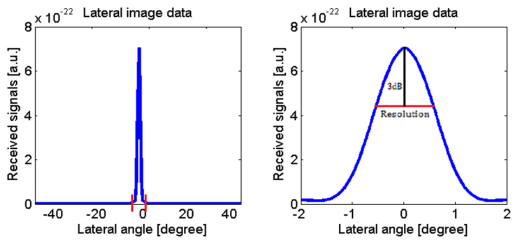

Fig. 5 Lateral image data of C-mode image of dense array (left) definition of side lobe, (right) definition of resolution

The image quality of three arrays are presented in Table 3. As aforementioned, the 2D dense array shows the best image quality. The case of the far field optimization is lower about 19% in ISLR, 57% in side lobe peak and 15% in side lobe sum than the case of the near field optimization. In terms of resolution, three arrays presents comparable performance.

Table 3 Comparison of three arrays

	Dense array	Far field optimization	Near field optimization
ISLR [dB]	-19.8	16.4	13.6
Side lobe peak [a.u.]	0.014	0.091	0.037
Side lobe sum [a.u.]	0.86	56.71	48.3
Lateral resolution [mm]	0.977	0.84	1.15
Axial resolution [mm]	0.236	0.236	0.236

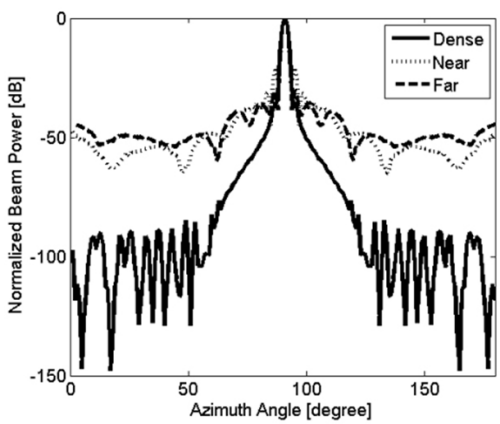

Fig. 6 Beam profile along the azimuth direction

In Fig. 6, the beam profiles along the azimuth direction (lateral direction) are presented. The beam profile shows the same result with Table 3 that the case of the near field optimization's side lobe level is lower than the case of the far field optimization. It is clearly presented that the sparse array can perform similar resolution around the main lobe, however, has higher side lobe level (40-50 dB) than the dense array (<80 dB). This higher side lobe level comes from less number of element (M=128) than that of the dense array (M=4096). As long as the distributed side lobe level is low enough, it will not significantly affect the image quality of the ultrasound images.

5. Conclusions

The 2D array is essential for 3D volumetric ultrasound imaging. However, implementation of the 2D dense array is challenging in terms of fabrication, interconnection and cabling. The 2D sparse array is realistic method for 3D images. The results shows that the 2D sparse array needs to be optimized for the operating range, not for the infinitely far target from the transducer array.

The optimized sparse array has comparable resolution to that of the dense array. However, it suffers from higher side lobe levels. Therefore, an acceptable level of side lobe needs to be defined that does not affect the image quality of the biological tissue. In addition, thermal noise as well as electrical noise needs to be considered for the realistic design of the 2D sparse array.

Acknowledgement

This research was supported by Basic Science Research Program through the National Research Foundation of Korea (NRF) funded by the Ministry of Science, ICT & Future Planning (No. 2014R1A1A1006024)

References

[1] P. K. Weber and L. Peter "1D and 2D Sparse Array Optimization," Instrumentation Science & Technology, Vol. 27, pp. 235-246 (1999)

[2] A. Austeng and S. Holm "Spare 2D arrays for real-time 3D ultrasound," *IEEE Trasactions On Ultrasonics, Ferroelectrics, and Frequency Control*, Vol. 49 pp. 1073-1086 (2002)

[3] J. W. Choe, O. Oralkan and P. T. Khuri-Yakub, "Design optimization for a 2-D sparse transducer array for 3-D ultrasound imaging," *Proceeding of the IEEE Ultrason. Symp*, pp. 1928-1931 (2010)

[4] B. Diarra, H. Liebgott, P. Tortoli and C. Cachard, "Sparse array techniques for 2D array ultrasound imaging," *Proceeding of the Acoustics 2012 Nantes Conference*, pp. 1591-1596 (2012)

[5] M. Karaman, I. O. Wygant, O. Oralkan and B. T. Khuri-Yakub, "Minimally redundant 2-D array designs for 3-D medical ultrasound imaging," *IEEE Transactions on Medical Imaging*, Vol. 28, pp. 1051-1061 (2009)

[6] A. Austeng and S. Holm, "Sparse 2-D arrays for 3-D phased array imaging-design method," *IEEE Trasactions on Ultrasonics, Ferroelectrics, and Frequency Control*, Vol. 49, pp. 2073-2085 (2002)

[7] Y. Jia, M. Xu, M. Ding and M. Yuchi, "3D ultrasound coherence imaging based on 2D array design," *Proceeding of the Medical Imaging 2013: Ultrasonic Imaging, Tomography, and Therapy* (2013)